XAS Study of Amorphous WO_3 Formation from a Peroxo-Tungstate Solution

T. Pauporté,*,† Y. Soldo-Olivier,‡ and R. Faure‡

Laboratoire d'Électrochimie et Chimie Analytique, UMR-CNRS 7575, Ecole Nationale Supérieure de Chimie, 11 rue P. et M. Curie, 75231 Paris Cedex 05, France, and Laboratoire d'Électrochimie et Physico-Chimie des matériaux et des Interfaces, UMR 5631-CNRS/INPG/UJF, 1130 rue de la Piscine, BP 75, 38402 Saint Martin d'Hères, France

Received: February 3, 2003; In Final Form: May 7, 2003

Electrodeposition is a low cost method for WO_3 thin film preparation. The starting dissolved tungsten precursor is a peroxo-compound which can be prepared by an equimolar mixing of sodium tungstate and hydrogen peroxide. The precursor preparation as well as the electrodeposition and precursor solution aging processes have been studied by X-ray absorption spectroscopy (XAS) at the W L_3 edge. By extended X-ray absorption fine structure (EXAFS) analysis, the local structure of the first oxygen octahedral shell around the W absorber has been characterized both in the colloidal oxide formed after deposition solution aging and in electrodeposited films. The colloidal compound could be fitted with the same procedure as that successfully used with a monoclinic WO_3 reference and involving two different W−O interatomic distances. The aging product is identified as amorphous WO_3. If the spectra of as-electrodeposited films could not be fitted by the same procedure, the structural parameters of those cycled electrochemically in a lithium ion containing organic medium have been determined. If compared to crystallized WO_3, the mean W−O distances in amorphous WO_3 (films and colloids) are found significantly shorter, whereas the Debye−Waller factors are much larger. The condensation process has been investigated by analyzing the variation of the X-ray absorption near edge structure (XANES) spectra. We show that the white line height of the W L_3 edge is a good indicator of the condensation state of the matter during the deposition. According to this parameter, the electrodeposited WO_3 films would undergo a dramatic reorganization process during the first potential cyclings in the lithium ion containing organic medium. The same behavior is observed with electrochromic films deposited by sputtering, a more classical method.

1. Introduction

WO_3 thin films have been the object of a considerable effort of research during the past two decades. They present especially interesting semiconducting[1,2] and electrochromic properties.[3] Some papers have described the successful electrodeposition of amorphous WO_3 films.[4−11] The method is based on the cathodic reduction of a peroxo-precursor which is obtained by mixing a tungsten precursor with hydrogen peroxide. In the previous works,[4−10] the preparation of this precursor was long and complicated. Moreover, the resulting solutions were reported unstable, their decomposition occurring after only 3−4 h of storage at room temperature. A first improvement was realized when it was shown that the addition of 30 vol. % alcohol (ethanol, 2-propanol, etc.) significantly increases the stability of these solutions.[5,6] Recently, one of us has reported a simplified method for the preparation of the peroxo-tungstate precursor and has emphasized the good stability in time of the resulting aqueous solutions.[11]

In the case of a precursor containing an equimolar ratio of W and $(O_2)^{2-}$, the precursor formulas was shown to be $WO_3(O_2)^{2-}$, with (O_2) a peroxide ligand.[11,12] The global deposition reaction is written

$$WO_3(O_2)^{2-} + (2 + x)\,H^+ + xe^- \Longrightarrow WO_3 + (2 + x)/2\,H_2O + (2 - x)/4O_2 \quad (1)$$

The films present the electrochemical signature of WO_3 when they are cycled in sulfuric acid or lithium perchorate organic solutions and good electrochromic properties (coloration efficiency, switching speed, etc.).[11]

In the present paper, we investigate the precursor solution preparation, the electrodeposition process, and the precursor solution aging at room temperature by the X-ray absorption spectroscopy (XAS) technique. We also emphasize the effect on these films of the first electrochemical cyclings in a lithium ion containing organic medium.

2. Experimental Section

The electrodeposited films (ed-WO_3) were synthesized at room temperature by the method described elsewhere.[11] The precursor deposition bath was prepared by mixing reagent grade 25 mM Na_2WO_4 (Acros organics 99%) plus 25 mM H_2O_2 (Prolabo, 30%) and acidifying at pH 1.3 by perchloric acid addition. The aged solution (col-WO_3) was obtained after storage during 15 days at room temperature. The deposition was carried out at −0.25 or 0 V versus NHE during 300 s. High purity carbon substrate (Toray Carbon Paper from E-Tek) was used.

* To whom correspondence should be addressed. E-mail: pauporte@ext.jussieu.fr.
† Ecole Nationale Supérieure de Chimie.
‡ UMR 5631-CNRS/INPG/UJF.

10.1021/jp034279s CCC: $25.00
Published on Web 07/19/2003

For the sake of comparison, 150 nm thick sputtered WO_3 thin films (sp-WO_3) deposited on the same carbon substrate were studied in parallel. The target was made of metal tungsten, the argon partial pressure was 2 Pa, the O_2 partial pressure was 2 or 3 Pa, and the flow was 18 cm^3 min^{-1}. The electrochemical cycling treatment consisted in five potential scans at 7 mV s^{-1} between 0.65 and −0.55 V vs NHE in a 0.3 M $LiClO_4$ (Fluka 99%) solution in propylene carbonate (Fluka). As a reference sample, we studied a crystallized monoclinic WO_3 powder (m-WO_3), heated several hours in air at 500°C. The structure of this compound was checked by X-ray diffraction (XRD). The solid samples were prepared as follows: 1 wt % of powder was mixed and ground with BN during a long time, prior to being pressed in order to obtain a 1 mm thick pellet. All of the experiments have been performed in air. No special attention was paid to control the experiment atmosphere composition.

The XAS spectra were acquired at the ID26 beamline of the European synchrotron radiation facility (ESRF-Grenoble-France). The electron energy in the storage ring was 6 GeV with an operating current ranging between 160 and 200 mA. The monochromator was a pair of parallel flat Si[111] single crystals. The photon flux at the sample was higher than 10^{13} ph s^{-1}. The spectra were recorded in the fluorescence mode. Two different detectors were used depending upon the sample investigated: a photodiode (powders, solutions) or a multi-element silicon drift detector (thin films). The spectra were recorded at the L_3 edge of the W absorber between 10 and 11.3 keV. Prior to spectrum comparison, the different curves were normalized. The background was removed by fitting the preedge by a straight line, and the postedge baseline was fitted by a cubic spline curve. The extracted EXAFS signal, $\chi(k)$, k being the wave vector, was multiplied by k^2, and a standard Kaiser window with parameter $\tau = 2$ was applied in order to minimize truncation effects. A Fourier transform (FT) of the resulting spectrum was calculated. This analysis was performed using the SEDEM software package written by D. Aberdam.[13] The theoretical backscattering phase and amplitude files were calculated by the FEFF 6.01 code[14] from the WO_2 structure in which the oxygen octahedra contain two different distances at 1.951 (4 atoms) and 2.062 Å (2 atoms).[15]

The first shells of oxygen atoms around the W absorber, isolated by FT, have been fitted with two different W−O interatomic distances and a set of structural parameters has been extracted for each distance with the help of the EXAFS formulas[16]

$$\chi(k) = \sum_i {S_0}^2 \frac{n_i}{k{r_i}^2} |f_i(k,\pi k)| \exp(-2k^2{\sigma_i}^2) \exp\left(-2\frac{r_i}{\lambda(k)}\right) \times \sin(2kr_i + \Psi_i(k)) \quad (2)$$

where the index i indicates the ith shell and n, r, and σ^2 refer to the neighbors number, the interatomic distance, and the Debye−Waller factor, respectively. $\lambda(k)$ is the electron mean free path, $f(k,\pi k)$ is the backscattering function, and $\Psi(k)$ is the total phase shift function. ${S_0}^2$ is an amplitude reduction factor due to many-body effects. As the basic unit of tungsten oxide compounds is a WO_6 octahedron, the total number of nearest oxygen neighbors was fixed at 6. This approach is quite simplified because, according to Loopstra et Rietveld,[17] two nonequivalent types of WO_6 octahedra would be present in m-WO_3 and each W−O distance in each octahedron would be different, giving a total of twelve different distances within the first shell. The electron mean-free path function, $\lambda(k)$, was calculated by the FEFF 6.01 code.[14] The prefactor ${S_0}^2$ was fixed at 0.8.

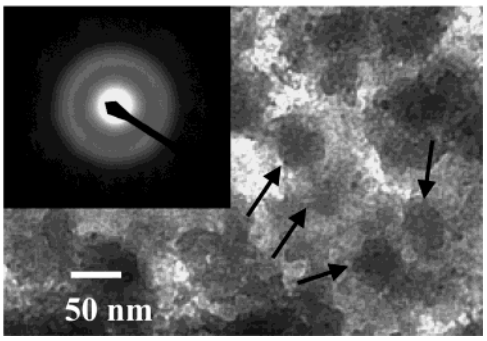

Figure 1. TEM view of the colloidal particles formed after 15 days of deposition solution aging. Inset: selected area diffraction pattern.

The colloidal product of the aged solutions was observed by transmission electronic microscopy (TEM). After ultrasonication during 15 min, a droplet of the solution was deposited onto a carbon grid and dried at air. The grids were observed with a 100 keV JEOL microscope.

3. Results

The decomposition-condensation process of peroxo-species occurs spontaneously in solutions stored at room temperature. In the case of a solution obtained by the mixing of sodium tungstate and hydrogen peroxide, this process is quite slow, and a white colored colloidal suspension appears after more than 10 days of storage (in the following, this solution is called colloidal or aged solution). TEM observation of the precipitated compound shows fine particles with a diameter in the 30−40 nm range (pointed out by some arrows in Figure 1). The electron diffraction pattern of these particles is a double halo ring without crystallite rings and shows a marked amorphous structure (inset in Figure 1). This pattern is similar to that reported for as-deposited sputtered films.[18] The condensation process can be accelerated electrochemically by applying a negative overvoltage by means of reaction 1. A conducting thin film is then formed on the electrode surface which is amorphous (no X-ray diffraction line). In a first step, we have determined by EXAFS analysis the short-range structural parameters of these two different amorphous compounds obtained from the same solution.

3.1. Structural Study of Colloidal and Thin Film Amorphous WO_3. Figure 2a shows the Fourier transform (FT) spectrum of the reference sample, analyzed over a large k range (2−14 $Å^{-1}$). Different peaks appear which have been indexed with help of the available literature data on XAS study of amorphous[19−21] and crystallized WO_3.[19−22] The first peak, in the distance interval of 0.8−1.9 Å, is ascribed to the first distorted shell containing 6 oxygen atoms. The second (2.3−3.1 Å) is attributed to multiple scattering processes within the first shell of the WO_6 octahedra. The third (3.1−4 Å) and the fourth (5−5.4 Å) peaks are assigned to the first and the second W−W coordination shell, respectively. The presence of the fourth peak confirms that the reference WO_3 sample was well-crystallized. Figure 2b shows the FT spectra obtained in the same k range with cycled ed-WO_3 and colloidal suspension. The second W−W distance is absent in these amorphous compounds. On the three different sample spectra, the first peak is divided into two subparts which suggests the presence of two main W−O distances in the first neighbor shells.

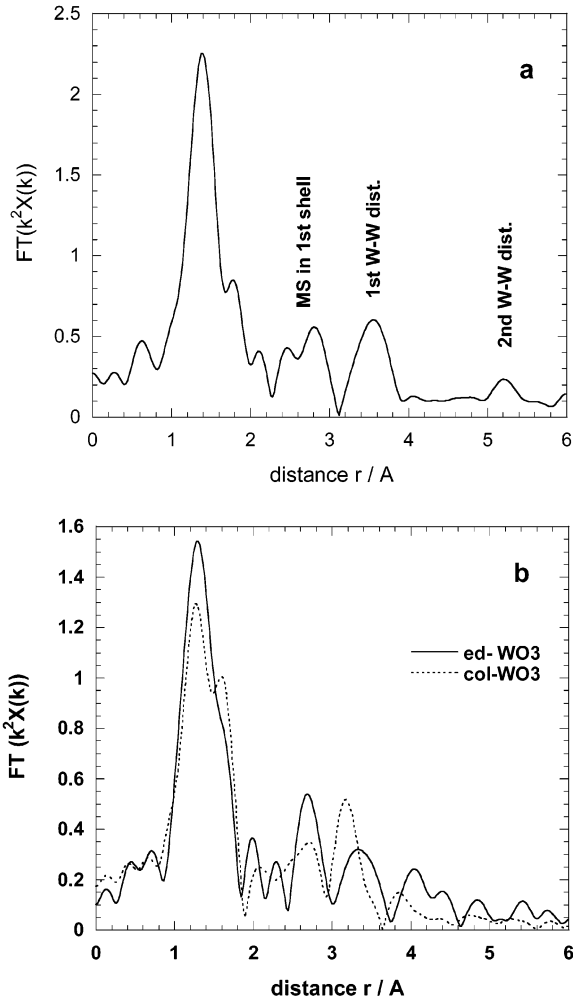

Figure 2. Fourier transform of $k^2\chi(k)$ spectra in the weighting window 2−14 $Å^{-1}$: a) m-WO_3; b) col-WO_3 (dotted line) and ed-WO_3 (full line).

The first peak was isolated between 0.86 and 2.02 Å, and an inverse-FT of the nearest oxygen neighbors contribution was calculated. The experimental curves are presented in Figure 3. They have been fitted with the EXAFS formulas (2) assuming the occurrence of two different W−O distances, r_1 and r_2. Figure 3 show that the fit obtained with the present method is satisfactory even if this approach is simplified (see the Experimental Section). The parameters of the local structure extracted by fitting are presented in Table 1. In Table 2 are summarized the mean W−O distances, $\bar{r}$ (defined as $(n_1r_1 + n_2r_2)/6$), in the first shell for the different samples. With m-WO_3, we find $\bar{r}$ at 1.93 Å, comparable to that reported by Purans et al.,[22] even if these authors fixed the number of nearest neighbors at 3 for each shell. We report σ^2 at 1.1×10^{-3} and 6.3×10^{-3} $Å^2$ for the two first shells respectively which are significantly lower than those found by these authors (Table 1). The Debye−Waller factor is related to the standard deviation σ, around the mean distance. It reflects the distribution of distances in a shell and, thus, the disorder in the compound. The interatomic distance dispersion described in the Experimental Section is included in the Debye−Waller Factor.

The EXAFS spectrum of the colloidal species in aqueous solution obtained by aging have been successfully fitted with the procedure described in the Experimental Section (Figure 3b). The parameters are presented in Tables 1 and 2. They suggest that the precipitate is made of amorphous WO_3. In the following, this compound is noted col-WO_3. Two main features

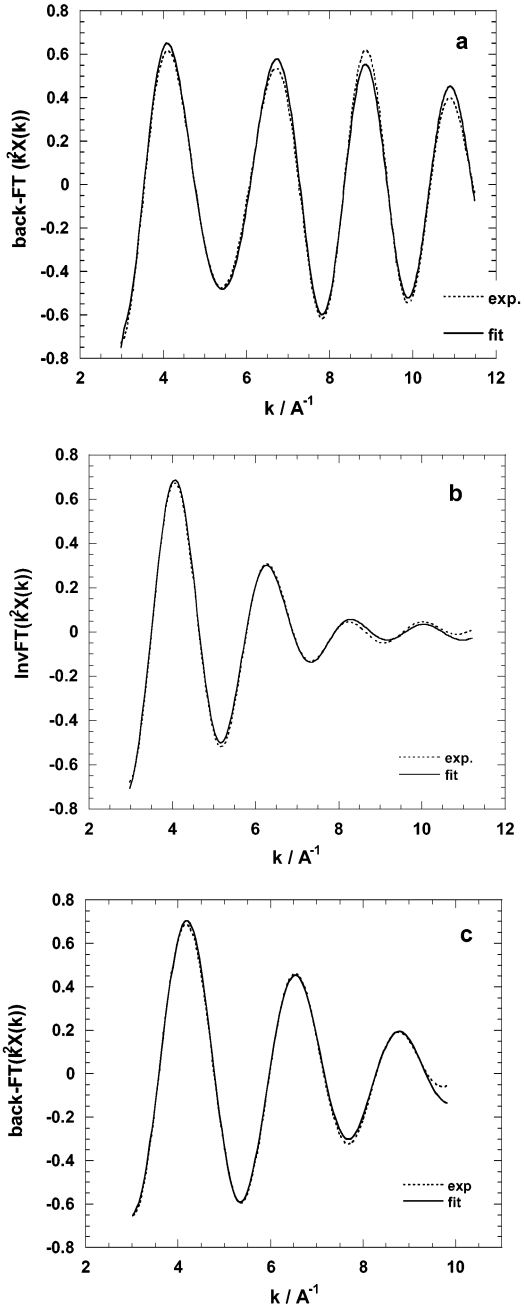

Figure 3. Inv-FT of the spectra after filtration of the first W−O coordination sphere contribution (r between 0.86 and 2.02 Å) (dotted line) and fit result (full line). (a) m-WO_3 (k range between 3 and 11.5 $Å^{-1}$), (b) col-WO_3 (k range between 3 and 11.5 $Å^{-1}$) and (c) ed-WO_3 (k range between 3 and 10 $Å^{-1}$).

are observed if compared to the reference sample: the mean interatomic distance steeply decreases, the new value being 1.83 Å, and the Debye−Waller factor associated to the first distance is markedly increased.

We failed to fit satisfactorily the EXAFS spectra of as-deposited tungsten oxide films by this procedure. However, the fitting was possible when the films were previously cycled in $LiClO_4$−PC medium. This effect and the local structure of the initial film will be studied in detail elsewhere.[23] We focus here on the EXAFS analysis of cycled films. An experimental spectrum, obtained after FT filtering is presented in Figure 3c. The structural parameters obtained by fitting are presented in Tables 1 and 2. The mean W−O distance lies between the two previous values, at 1.87 Å. The other main feature is the high

TABLE 1: Local Structure around Tungsten in m-WO_3, col-WO_3, and ed-WO_3 Determined by EXAFS[a]

sample	subshell	r/Å.	n	σ^2 ($\times 10^3$)/Å^2	dE0 /eV	ref
m-WO_3	1	1.79	3	3.32		17
	2	2.09	3	11		
m-WO_3	1	1.80	3.2	1.1	9.7	this study
	2	2.09	2.8	6.3	9.5	
col-WO_3	1	1.72	2.0	8.0	11.9	
	2	1.88	4.0	8.8	2.5	
ed-WO_3	1	1.79	3.6	7.8	7.9	
	2	1.98	2.4	26.1	0.81	

[a] r_i is the W−O interatomic distance, n_i is the coordination number with $n_1 + n_2 = 6$, and σ^2 is the Debye−Waller factor. In the present analysis, the k range was 3−11.5 Å^{-1} for m-WO_3 and col-WO_3, and 3−10 Å^{-1} for ed-WO_3. The first coordination shell was isolated between 0.86 and 2.02 Å from the Fourier transform of the experimental EXAFS spectra.

TABLE 2: Mean Interatomic W−O Distance in the First Coordination Shell

sample	method	$\bar{r}^a$/Å	ref
m-WO_3	EXAFS	1.94	17
	XRD	1.93	
m-WO_3	EXAFS	1.93	this study
ed-WO_3		1.87	
col-WO_3		1.83	

[a] Mean distance defined as $(n_1r_1 + n_2r_2)/6$

Debye−Waller factor for the second distance at 26 $\times$ 10^{-3}Å^2. As expected, the disorder is much higher in this compound compared to the crystallized powder.

We report that $\bar{r}$ is significantly shorter in amorphous WO_3 as compared to m-WO_3. It has been shown elsewhere that the metal−oxygen interatomic distance in oxide can vary with the oxidation state of the metal.[24,25] This effect cannot be invoked here because W in amorphous ed-WO_3 films are in the oxidized colorless state, the same as in the reference sample. A likely explanation is the presence of short W═O terminal bonds in the amorphous compounds.[26]

3.2. XANES Study of WO_3 Formation. The experimental X-ray absorption spectra at the W L_3 edge of m-WO_3, Na_2WO_4, different precursor solutions, and films present a peak above the absorption edge energy centered at 10 210−10 215 eV. This strong resonance is called the white line (WL) and is attributed to the transition of the photoelectron between $2p_{3/2}$ level and a final state in the continuum with 5d atomic character.[21]

We have measured the XANES spectra of various samples in relation to the electrodeposition of WO_3. A first series of result deals with the precursor solution (Figure 4). Figure 4a shows the effect of Na_2WO_4 salt dissolution on the XANES spectrum. It appears that the white line height (WLH) markedly increases from 2.81 to 3.58 with dissolution. The energy of the edge, E_0, (measured at the edge inflection point) remains unchanged at 10 208.5 eV. The solubilization is thus not accompanied by a spontaneous change of the W oxidation state. These measurements emphasize the marked influence of the environment on the WLH.

Figure 4b shows the effect of hydrogen peroxide addition and acidification by perchloric acid on the absorption edge shape. The WLH parameter and E_0 remain almost unchanged between these two solutions. W is thus not oxidized by H_2O_2, and its oxidation state in the precursor compound remains at ca. +VI. This is in agreement with the literature data on the peroxo-tungstate species formed in these conditions[12] and with our previous EQCM observations.[11] In the case of an equimolar mixing of Na_2WO_4 and H_2O_2, the reaction is fast and complete and the precursor has been described as $W(O_2)O_3^{2-}$.[11]

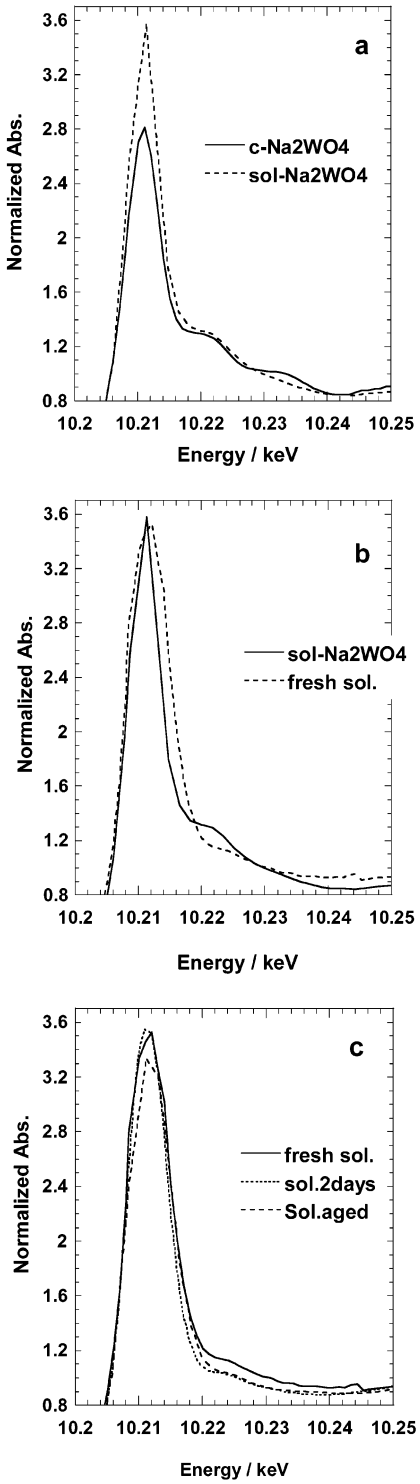

Figure 4. W L_3 edge XANES spectra of different samples related to the deposition solution: (a) effect of Na_2WO_4 dissolution (solid line, powder; dotted line, 25 mM solution in water), (b) effect of peroxide addition and acidification (solid line, Na_2WO_4 solution; dotted line, fresh deposition solution), and (c) effect of storage time on the deposition solution.

A drawback of the electrodeposition from peroxo precursor method is the usual lack of stability of the deposition bath. In Figure 4c is presented the effect of solution aging at room temperature on the XANES spectra. The figure shows that, after 2 days of storage at room temperature, the XANES spectrum

TABLE 3: Summary of the Various Samples Investigated by XANES[a]

sample	no.	WL heigth	condensation degree[b]
WO_3 crystallized	1	3.04	6
ed-WO_3[c]cycled in Li−PC	3	3.00	
sp.-WO_3[d]cycled in Li−PC	4	3.02	
aged deposition solution	5	3.34	3
ed- WO_3[c]	6	3.41	2
sp.-WO_3[d]	7	3.41	
solubilized Na_2WO_4	8	3.58	1
fresh deposition solution	9	3.53	
deposition sol. Stored 2 days	10	3.55	

[a] White Line Height Values Calculated after normalization. [b] Scale arbitrarily set from 1 to 6. [c] Film electrodeposited at −0.25V vs NHE. [d] Film deposited by sputtering.

does not evolve. This confirms the good stability in time of the present deposition solutions as also observed elsewhere by EQCM.[11]

The colloidal precipitation product described above shows a WLH parameter significantly lower than that of the starting solution with a value of 3.34 (Table 3). In fact, this parameter lies between the values measured for a crystallized WO_3 reference and a fresh deposition solution (Table 3) even if we have shown that the aging product is most likely amorphous WO_3 fine particles.

Solid compounds have also been investigated (Figure 5). For ed-WO_3 films deposited on a carbon substrate at two different potentials, the WLH is independent of the deposition potential with a value of 3.41 (Figure 5a). For the sake of comparison, we also report a XANES spectrum of a thin film of amorphous WO_3 deposited by sputtering, a more conventional method for electrochromic WO_3 thin film preparation. The initial WLH is the same (Figure 5b). A dramatic effect on WLH is induced by the electrochemical cycling of these two kinds of films in $LiClO_4$/PC. The height falls from 3.4 down to a value close to that of crystallized monoclinic WO_3, that is 3.0. The E_0 parameter is not affected by this treatment and accordingly, the oxidation state of W is unchanged.

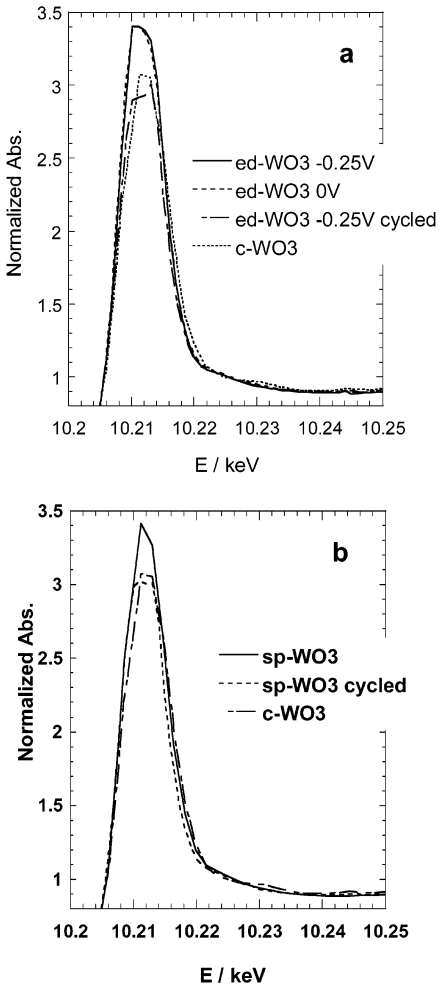

Figure 5. Effect of film cycling on W L_3 edge XANES spectra and comparison with the crystallized m-WO_3 reference. (a) Films deposited by electrodeposition at two different potentials; (b) film deposited by sputtering.

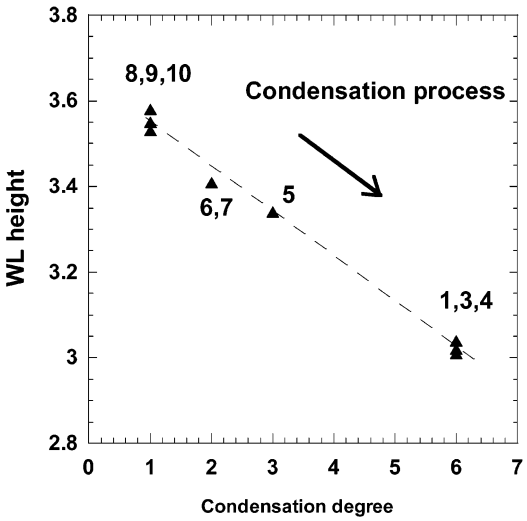

Figure 6. Variation of the white line height at the W L_3 edge with the condensation degree (the point labels correspond to the sample numbered in Table 3).

4. Discussion

A large variety of samples have been investigated by XANES, from the dissolved tungsten precursor salt to cycled WO_3 thin films and a crystallized reference. We have shown that if they all contain W in an oxidation state of ca. +VI, their WLH surprisingly varies in a very large range. The results are summarized in Table 3. In Table 3, we also settle an arbitrary scale which reflects the variation of the WLH parameter by a rough linear behavior. Figure 6 displays the different points and emphasizes the very large variation of WHL from one sample to another. This figure reveals that this parameter is markedly decreased, first, after the WO_3 deposition or condensation process and, second, after the film cycling in the organic $LiClO_4$ medium. It is noteworthy that the general effect observed is the inverse to that described above during the solubilization of Na_2WO_4 (Figure 4a). In general, this behavior seems to be closely related to the condensation degree of the W species (that we can also qualify as the middle range order) in the sample. One may also suggests that the key parameter governing the WLH could be the hydration level. To test this hypothesis, the O/W atomic ratios in ed-WO_3 and sp-WO_3 films have been determined. The tungsten content was obtained by Rutherford backscattering spectrometry of $\alpha(^4He^+)$ particles at 2 MeV, whereas the oxygen content was determined directly by the nuclear reaction $^{16}O(d,p)^{17}O$. We found the O/W ratio to be 2.8 in sp-WO_3 films and 3.45−3.50 in films deposited between −0.25 and 0 V vs NHE.[23] These latter values suggest that electrodeposited films would contain some water and have the general formulas $WO_3 \cdot 1/2\ H_2O$. On the contrary, sputtered films

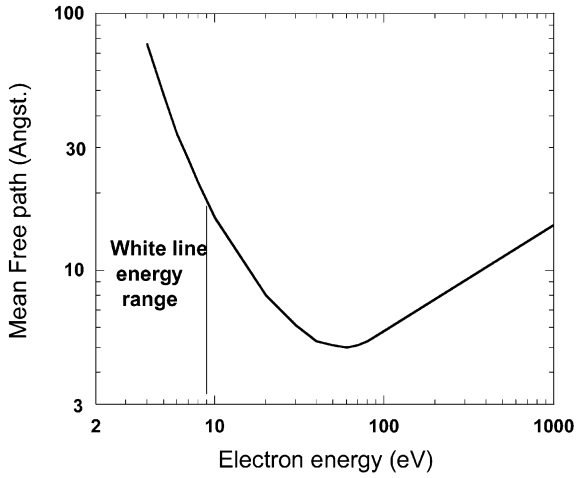

Figure 7. General curve for the electron mean free path as a function of the electron energy. The energy range where we observe the white line height variations is shown.

are water-free. Despite this difference in hydration, they present the same WLH. Accordingly, WLH is instead an indicator of the condensation level of the W species rather than hydration level.

This hypothesis is supported by the kinetic properties of the photoelectron which is used as a local probe in XAS technique. Figure 7 shows a general curve of the electron mean free path as a function of the electron energy.[27] In the energy region of the white line, $\lambda(E)$ values are larger than 20 Å. XANES behavior and hence WLH are thus quite sensitive to the structural arrangement at a middle distances. A similar sensitivity to the middle range order has been shown for instance by Bianconi at the K edge of Cu.[28]

The WLH is thus a convenient tool to estimate the condensation degree of a compound. Figure 6 reveals that the first potential cycle scans play an important role in the structural condensation and reorganization of the films. This is observed with either films deposited electrochemically or by sputtering. From Figure 6, we can also state that the colloids obtained by solution aging are likely more condensed than the as-deposited amorphous thin films.

5. Conclusions

We have discussed the two different condensation routes of peroxo-precursor in aqueous solutions which are aging and cathodic electrodeposition. Different method analyses show that the colloid product obtained by precursor solution aging is likely nanoparticles of amorphous WO_3. The thin films electrodeposited cathodically and subsequently cycled electrochemically in organic lithium perchlorate medium are identified unambiguously as amorphous WO_3.

By the analysis of the EXAFS signal recorded at the W L_3 edge, we have determined the structural parameters of the first oxygen shell around the W absorber of the two different amorphous WO_3 oxides. We show that the W−O mean distance is longer in crystallized WO_3 reference sample if compared to amorphous ones. The mean W−O bond is shorter in colloidal WO_3, in comparison to thin films. The disorder, measured by the Debye−Waller factor, is higher in amorphous compounds as compared to the crystallized one. The precursor solution preparation and the deposition mechanism have been studied by XANES at the W L_3 edge. The study shows that W is in a +VI oxidation state in the deposition precursor which has been described as $W(O_2)O_3^{2-}$ when it results from an equimolar mixture of Na_2WO_4 and H_2O_2. The good stability in time of this precursor has been confirmed.

The investigation of a large variety of species containing W in an oxidation state of ca. +VI suggests that the white line height is a good indicator of the condensation degree of the W species. From this parameter, we find that the WO_3 colloidal particles are more condensed than the oxide deposited electrochemically as a film. The WLH variations also reveals that the first potential cycles in $LiClO_4$/PC medium likely dramatically affect the organization and local condensation degree of the WO_6 octahedra, the elemental units of tungsten oxide compounds. More generally, the present study open new perspectives for the investigation of condensation phenomena in wet medium which are largely used for the synthesis of a wide variety of compounds. Of special interest are the electrochemically induced condensation of peroxo-precursors leading to the deposition of TiO_2, MoO_3, IrO_2, RuO_2, etc.[29] or sol−gel synthesis (condensation of tungstates, molybdates, vanadates, etc. by pH and concentration monitoring).[30]

Acknowledgment. P. E. Petit (ESRF, Grenoble, France) and the staff of the ID26 beamline are acknowledged for XAS experiments. M. C. Bernard and F. Pillier (UPR15, University of Paris VI, France) are thanked for the RBS, TEM, and SAD experiments. A. Billard (LSGS, École des mines, Nancy, France) is acknowledged for thin film preparation by sputtering and P. Mandin (LECA, ENSCP, Paris, France) for his help in data file processing.

References and Notes

(1) Shiyanovskaya, I.; Hepel, M. *J. Electrochem. Soc*. **1999**, *146*, 243.
(2) Kang, T.-S.; Moon, S.-H.; Kim, K−J. *J. Electrochem. Soc.* **2002**, *149*, E155.
(3) Granqvist, C. G. *Handbook of Inorganic Electrochromic Materials*; Elsevier: Amsterdam, 1995.
(4) Dao, L. H.; Guerfi, A.; Nguyen, M. T. in *Electrochromic Materials*, M. C. Carpenter and D. A. Corrigan, Editors, Vol. 90−2, The Electrochemical Society Proceedings Series, Pennington, NJ, 1990; p30.
(5) Shen, P. K.; Syed-Bokhari, J.; Tseung A. C. C. *J. Electrochem. Soc*. **1991**, *138*, 2778.
(6) Shen, P. K.; Tseung, A. C. C. *J. Mater. Chem.* **1992**, *2*, 1141.
(7) Pennisi, A.; Simone, F.; Lampert, C. M. *Sol. Ener. Mater. Sol. Cells* **1992**, *28*, 233.
(8) Monk, P. M. S.; Chester, S. L. *Electrochim. Acta* **1993**, *38*, 1521.
(9) Meulenkamp, E. A. *J. Electrochem. Soc.* **1997**, *144*, 1664.
(10) Meulenkamp, E. A.; De Groot, R. J. J.; de Vries, J. M. L *Mater. Res. Soc. Symp. Proc.* **1997**, *451*, 321.
(11) Pauporté, T. *J. Electrochem. Soc*. **2002**, *149*, C539.
(12) Connor, J. A.; Ebsworth, E. A. V. *Inorg. Chem. Radiochem*. **1964**, *6*, 279.
(13) Aberdam, D. *J. Synchrotron Rad*. **1998**, *5*, 1287. The package can be downloaded from the ESRF website (www.esrf.fr).
(14) Rehr, J. J.; Mustre de Leon, J.; Zabinsky, S. I.; Albers, R. C. *J. Am. Chem. Soc.* **1991**, *113*, 5135.
(15) Wyckoff, R. W. G. *Crystal Structure*, 2nd ed.; Interscience Publisher: New York, 1964; Vol. 1, Chapter 4, p 250.
(16) Koeningsberger, D. C.; Prins, R. *X-ray Absorption: Principles, Application, Technique of EXAFS, SEXAFS and XANES*; Wiley: New York, 1988; p 45.
(17) Loopstra, B. O.; Rietveld, H. M. *Acta Crystallogr. B* **1969**, *25*, 1420.
(18) Wang, X. G.; Jiang, Y. S.; Yang, N. H.; Yuan, L.; Pang, S. J. *Appl. Surf. Science* **1999**, *143*, 135.
(19) Balerna, A.; Bernieri, E.; Burattini, E.; Kuzmin, A.; Lusis, A.; Purans, J.; Cikmach, P. *Nucl. Instr. Methods Phys. Res.* **1991**, *A308*, 234.
(20) Balerna, A.; Bernieri, E.; Burattini, E.; Kuzmin, A.; Lusis, A.; Purans, J.; Cikmach, P. *Nucl. Instr. Methods Phys. Res.* **1991**, *A308*, 239.
(21) Kuzmin, A.; Purans, J. *J. Phys.: Condens. Matter* **1993**, *5*, 2333.
(22) Purans, J.; Kuzmin, A.; Guéry, C. *Proc. SPIE, Int. Soc. Opt. Ing.* **1997**, *968*, 174.

(23) Pauporté, T.; Bernard, M. C.; Soldo-Olivier, Y.; Faure, R. submitted.
(24) Pauporté, T.; Aberdam, D.; Hazemann, J. L.; Faure, R.; Durand R. *J. Electroanal. Chem*. **1999**, *465*, 88.
(25) Mo, Y.; Antonio, M. R.; Scherson, D. A. *J. Phys. Chem. B* **2000**, *104*, 9777.
(26) Daniel, M. F.; Desbat, B.; Lassegues, J. C.; Gerand, B.; Figlarz, M. *J. Solid. State Chem*. **1987**, *67*, 235.
(27) Teo, B. K. *EXAFS: Basic Principles and Data Analysis*; Springer: Berlin, 1986; p 92.
(28) Bianconi, A. *Topics in Current Chemistry*; Springer-Verlag: Berlin 1988; Vol. 145, p 29.
(29) Therese, G.; Kamath, P. V. *Chem. Mater*. **2000**, *12*, 1195.
(30) Jolivet, J. P., *De la Solution a l'Oxyde*; Interedition-CNRS edition: Paris, 1994.